# Nanostructured copper-zirconia composites as catalysts for methanol decomposition

Tanya Tsoncheva[a,*], Izabela Genova[a], Momchil Dimitrov[a], Eva Sarcadi-Priboczki[b], Anna Maria Venezia[c], Daniela Kovacheva[d], Nicola Scotti[e], Vladimiro dal Santo[e]

[a] *Institute of Organic Chemistry with Centre of Phytochemistry, Bulgarian Academy of Sciences, Sofia, Bulgaria*
[b] *Institute of Nuclear Research, Hungarian Academy of Sciences, Debrecen, Hungary*
[c] *CNR-Istituto per lo Studio dei materiali Nanostrutturati Via Ugo La Malfa 153, 90146 Palermo, Italy*
[d] *Institute of General and Inorganic Chemistry, Bulgarian Academy of Sciences, 1113 Sofia, Bulgaria*
[e] *CNR - Istituto di Scienze e Tecnologie Molecolari, via C. Golgi 19, 20133 Milano, Italy*

*Keywords:*
Methanol decomposition
Mesoporous $ZrO_2$
Copper modifications

A B S T R A C T

Nanostructured mesoporous $ZrO_2$ was obtained by hydrothermal synthesis using surfactant assisted approach. Copper modifications of thus obtained $ZrO_2$ (4–25 wt.% copper) were prepared by incipient wetness impregnation with the corresponding nitrate or acetyl acetonate precursors and further treatment in oxidative or reduction atmosphere. The obtained materials were characterized by $N_2$ physisorption, XRD, UV–vis, FTIR, XPS and temperature programmed reduction with hydrogen and tested as catalysts in methanol decomposition to hydrogen and CO. Selected samples were investigated after partial coverage of the surface with $^{11}C$-labeled methanol and $^{11}C$-labeled methyl formate. The formation of monolayer of finely dispersed copper oxide species on zirconia at about 4 wt.% copper loading and bulk copper nanoparticles at higher one is observed. It was assumed that zirconia support provides the formation of two types of catalytic sites: the first ones strongly adsorb methanol and exhibit predominantly dehydrogenation activity, while the others, possess acidic function. The modification of zirconia with copper significantly improves the catalytic activity and selectivity in methanol decomposition *via* (i) creation of additional surface acidic sites which contribute to generation of methoxy intermediates; (ii) stabilization of $Cu^{2+}$-$Cu^{+}$ and $Cu^{+}$-$Cu^{0}$ redox pairs where the electron transfer is facilitated by zirconia support and (iii) assisting the recombination and release of hydrogen during the transformation of produced on zirconia surface intermediates.

## 1. Introduction

The properties of zirconia, namely, high strength and hardness, good elastic modulus, corrosion resistance, biocompatibility, and high melting temperature make the material interesting for applications as advanced ceramics in bio-sensors, piezoelectric devices, oxygen sensors, abrasives, as well as catalysts, catalyst support or promoters [1-9 and refs. therein]. Meanwhile, zirconia doped with copper oxides receive great attention as anode materials for solid oxide fuel cells [10] and catalysts for methanol synthesis [11–13], carbon monoxide oxidation [14], NO reduction with hydrocarbons or CO [15], water–gas-shift reaction [16,17], methanol reforming [18], CO and $CO_2$ hydrogenation [19]. The advantages of using zirconia as a catalyst support originates from its strong interaction with the active phase, high thermal stability, and unique combination of acidic, basic, and redox ability [20]. Broensted acidic and basic hydroxyl groups and co-ordinatively unsaturated Lewis acid–base $Zr^{4+}$–$O^{2-}$ pairs [19 and refs. therein] were simultaneously detected on zirconia surface. The surface properties of zirconia strongly depend on zirconia polymorphs. Hertl [21] suggested that tetragonal zirconia possessed high basicity, while monoclinic zirconia had relatively high Lewis and Broensted acidity. It was established [19] that during the catalysts preparation, surface properties of zirconia polymorphs impacted the interaction between copper and zirconia leading to higher dispersion of copper on tetragonal $ZrO_2$ support. The authors [19] observed also higher catalytic activity in methanol synthesis for copper modified tetragonal $ZrO_2$ than the amorphous and monoclinic modifications. $ZrO_2$ polymorphs could be tuned with addition of certain divalent or trivalent cations or by decreasing the crystallite size below a critical value [22,23]. Nowadays, advanced technologies, such as sol–gel, chemical vapor synthesis, combustion and precipitation procedures have been

developed to produce nanopowder zirconia [24–26]. Among them, hydrothermal process is reported to be a soft chemical route to prepare phase pure products at low temperature and easy control of crystal size by altering the process conditions [7 and refs therein]. Recently, much attention was paid to the synthesis of nanostructured mesoporous oxides with high surface area and uniform pore size distribution using a surfactant-assisted route [27,28 and refs therein].

Hydrogen production is one of the most important technologies for the chemical industry, power generation and fuel cell application [29]. Instead of handling $H_2$ under high-pressure or cryogenic conditions, hydrogen can be produced on board by catalytic steam reforming of natural gas and oil-derived naphtha, and partial oxidation of heavy oils. Nevertheless, these technologies are developed enough into market value, the depletion of fossil fuels and the large quantity of $CO_2$ emissions focused recently the attention on biomass as renewable, environmentally friendly feedstock with no contribution to a net increase in atmospheric carbon dioxide [30]. Methanol, which can be produced from biomass, is regarded as an attractive alternative fuel, also for portable power systems, due to the low temperature of hydrogen release and higher specific energy than either lithium batteries or stored hydrogen [31–33]. Hydrogen can be obtained from methanol through various techniques such as simple decomposition, steam-reforming, partial oxidation and oxidative steam reforming [34–36]. Number of recent studies assumed that copper and zirconia behaved in a bi-functional manner during the methanol decomposition or methanol synthesis, with Cu serving as a site for the dissociation or removal of hydrogen molecules, and zirconia as an adsorption site for carbon containing intermediates [17,37–39 and refs therein]. However, in spite of such bi-functional roles of copper and $ZrO_2$, the influence of the intrinsic nature of each component on the beneficial synergy between them is not yet well understood. The aim of current paper is to highlight the effect of composition and preparation procedure of nanosized copper-zirconia composites on their catalytic behavior in methanol decomposition. The elucidation of mechanism of the reaction and the role of different catalytic sites is also in the scope of the study using original catalytic $^{11}C$-radiolabeling approach. Nanodispersed mesoporous $ZrO_2$ was obtained by surfactant-assisted procedure and used as a catalyst support. The copper loading was varied in a wide range by incipient wetness impregnation of $ZrO_2$ with aqueous solutions of copper nitrate. Alternatively, selected samples were obtained by molecular design dispersion method (MDD) by anchoring of copper acetyl acetonate to the zirconia surface hydroxyl groups [40,41]. In order to study the specific role of copper and zirconia as well as the synergy between them thus obtained materials were compared with some copper modifications of ordered mesoporous SBA-15 silica. A complex of conventional physicochemical techniques, such as $N_2$ physisorption, XRD, UV–vis, FTIR, XPS and TPR was applied for catalysts characterization.

## 2. Experimental

### 2.1. Materials

The synthesis of the nanostructured zirconia was achieved by template-assisted approach according to the procedure reported in [42]. In principle, 6.0 g N-hexadecyl-N,N,N-trimethylammoniumbromide (CTAB) were dissolved in 50 ml distilled water. To this solution was added slowly and under vigorous stirring a solution of $ZrCl_4$ (3.40 g) in 25 ml distilled water. Then, the temperature was raised to 323 K and the reaction mixture was stirred for 30 min before adding drop-wise 20 ml $NH_4OH$ (12.5%). The resulting mixture was stirred overnight at 323 K. Then it was transferred into a polypropylene container and heated at 373 K for 24 h. The so-prepared particles were then filtrated, washed with distilled water, then dried at room temperature and extraction of the organic template in absolute ethanol (100 ml per 1 g carrier) was conducted at 343 K for 24 h under reflux conditions. Then, the sample was filtrated and dried at room temperature before calcination in air with a ramp of 1 K/min and dwelling time of 6 h at 473, 573 and 673 K. The mesoporous SBA-15 silica was prepared according to the procedure described in [43] using Pluronic 123 as a structure directing agent. The template was released by calcination for 6 h at 773 K. The zirconia modifications with nominal copper content of 4, 8, 12 and 25 wt.%, were prepared by wet impregnation of $ZrO_2$ support with aqueous solution of copper nitrate. After drying, the samples were calcined in air at 673 K for 2 h and denoted as $n$Cu/$ZrO_2$(N,o) where $n$ was the nominal copper loading in wt.%. Selected samples were additionally reduced in hydrogen at 523 K for 2 h and denoted as $n$Cu/$ZrO_2$(N,r). The reference SBA-15 silica based materials, treated in air, $n$Cu/SBA-15(N,o), or in air and hydrogen, $n$Cu/SBA-15(N,r), were prepared following the same procedure. The copper content of the samples, determined by Atomic Absorption Spectroscopy was presented in Table 1. Alternatively, the samples denoted as 4Cu/$ZrO_2$(A,o) and 8Cu/$ZrO_2$(A,o) were prepared by impregnation of $ZrO_2$ with toluene solution of copper acetyl acetonate. After the decomposition of acetyl acetonate precursor in air at 673 K (1 K/min) for 2 h, materials containing 4.3 and 7.8 wt.% Cu were obtained.

### 2.2. Methods of investigation

Copper content in the samples was determined by Atomic Absorption Spectroscopy on an Atomic Absorption Spectrometer 3100 – Perkin-Elmer; flame: acetylene/air. Specific surface area and pore size distribution were measured through nitrogen adsorption–desorption isotherms at 77 K using a Quantachrome NOVA 1200 apparatus. $S_{BET}$ was calculated applying the Brunauer, Emmet and Teller (BET) equation for $N_2$ relative pressure in range of $0.05 < P/P_0 < 0.30$. Pore size distribution was determined by DFT method from the desorption branch of the isotherm. Powder X-ray diffraction patterns were on a Bruker D8 Advance diffractometer with Cu $K_\alpha$ radiation and using a LynxEye detector. The average crystallite size was evaluated according to Scherrer equation. The UV–vis spectra were recorded on a Jasco V-650 UV–vis spectrophotometer equipped with a diffuse reflectance unit. FTIR spectra in the region of skeletal vibrations were recorded on a Bruker Vector 22 spectrometer at a resolution of 1–2 $cm^{-1}$, accumulating 64–128 scans and KBr pellets technique. The pyridine desorption spectra were carried out with a BioRad FTS-60 spectrophotometer equipped with mid-IR MCT detector. The experiments were performed on sample disk (15–20 mg) after a pre-treatment (dehydration under vacuum at 383 K for 1 h or reduction at 523 K under $H_2$ for 2 h). One spectrum was collected before probe molecule adsorption as a blank experiment, then pyridine (Py) vapors were adsorbed on the disk at room temperature and following desorption steps (30 min, vacuum, every 50 K) were performed from RT to 523 K. The spectra were collected after each desorption step after cooling the sample. The X-ray photoelectron spectroscopy (XPS) analyses were performed with a VG Microtech ESCA 3000 Multilab, equipped with a dual Mg/Al anode. The spectra were excited by the unmonochromatised Al Kα source (1253.6 eV) run at 14 kV and 15 mA. The analyzer operated in the constant analyzer energy (CAE) mode. Survey spectra were measured at 50 eV pass energy. For the individual peak energy regions, a pass energy of 20 eV set across the hemispheres was used. The sample powders were mounted on a double-sided adhesive tape. The pressure in the analysis chamber was in the range

**Table 1**
Samples composition and nitrogen physisorption data (specific surface area – $S_{BET}$, total pore volume – $V_{tot}$, and average pore diameter – $D$) for various modifications. For comparison, data for the SBA-15 modifications are also presented.

| Sample | Support | Cu, wt.% | $S_{BET}$, $m^2/g$ | $V_{tot}$, $cm^3/g$ | $D$, nm |
|---|---|---|---|---|---|
| $ZrO_2$ | $ZrO_2$ (m-70%; t-30%)* | – | 127 | 0.33 | 8.2 |
| 4Cu/$ZrO_2$(N,o) | $ZrO_2$ (m-80%; t-20%) | 4.0 | 118 | 0.32 | 8.2 |
| 8Cu/$ZrO_2$(N,o) | $ZrO_2$ (m-82%; t-18%) | 7.3 | 113 | 0.29 | 8.2 |
| 12Cu/$ZrO_2$(N,o) | $ZrO_2$ (m-84%; t-16%) | 10.9 | 106 | 0.25 | 8.1 |
| 25Cu/$ZrO_2$(N,o) | $ZrO_2$ (m-81%; t-19%) | 21.3 | 87 | 0.21 | 8.5 |
| SBA-15 | SBA-15 | | 845 | 1.21 | 6.4 |
| 4Cu/SBA-15(N,o) | SBA-15 | 4.4 | 555 | 0.83 | 6.4 |
| 8CuO/SBA-15(N,o) | SBA-15 | 9.0 | 573 | 0.88 | 6.0 |

* m – monoclinic $ZrO_2$; t – tetragonal $ZrO_2$.

of $10^{-8}$ Torr during data collection. The constant charging of the samples was corrected by referencing all the energies to the C 1s peak energy set at 285.1 eV, arising from adventitious carbon. Analyses of the peaks were performed with the software provided by VG. Atomic concentrations were calculated from peak intensity using the sensitivity factors included in the software. The binding energy values are quoted with a precision of ±0.15 eV and the atomic percentage with a precision of ±10%. The TPR/TG (temperature-programmed reduction/thermo-gravimetric) analyses were performed on a Setaram TG92 instrument in a flow of 50 vol% $H_2$ in Ar (100 $cm^3$ $min^{-1}$) and heating rate of 5 K $min^{-1}$. The hydrogen consumption TPR profiles were recorded with a modified Micromeritics Pulse Chemisorb 2700 apparatus equipped with a thermo conductivity detector. Before the measurements, the samples were calcined at 773 K under $O_2$ (40 ml/min) and then reduced with a mixture of 8% $H_2$ in Ar (15 ml/min) with a heating rate of 8 K/min.

### 2.3. Catalytic tests

#### 2.3.1. Methanol decomposition in a flow type system

Methanol conversion was carried out in a flow reactor (0.055 g of catalyst), argon being used as a carrier gas (50 $cm^3$ $min^{-1}$). The methanol partial pressure was 1.57 kPa. The catalysts were tested under conditions of a temperature-programmed regime within the range of 350–770 K with heating rate of 1 K $min^{-1}$. Before the catalytic test calcined samples were treated under Ar flow at 373 K for 1 h. Selected samples were subjected under the *in-situ* reduction in a flow of $H_2$ and Ar (1:1) at 523 K for 2 h. On-line gas chromatographic analyses were performed on HP apparatus equipped with flame ionization and thermo-conductivity detectors, on a PLOT Q column, using an absolute calibration method and a carbon based material balance. The product selectivity was calculated as $Yi/X \times 100$, where $Yi$ was the yield of the $i$ product (calculated as detected amount of $i$ product/initial amount of methanol, before the introduction in the catalytic reactor) and $X$ was the methanol conversion at selected temperature. Specific activity (SA) was calculated as $X/m_i$ where $X$ and $m_i$ were the conversion at 650 K and copper content in the sample (wt.%), respectively.

#### 2.3.2. $^{11}$C-methanol and $^{11}$C-methyl formate conversion

$^{11}$C-methanol radiolabeling experiments were done in a closed static reactor and the analyses were performed on HP 6890 GC equipped with a PLOT Q column, flame ionization detector (FID) and radioisotope detector BIOSCAN Flow-Count (RD). The reduction of the samples was performed *in-situ* in a flow of $H_2$ and Ar (1:1) at 523 K for 2 h. The catalytic experiments were carried out after preliminary coverage of the catalyst surface with $^{12}$C- and/or $^{11}$C-methanol or $^{11}CH_3OCHO$ (MF) according to the following adsorption procedures:

(A) $^{11}CH_3OH$ adsorption at 333 K, heating to 373 K and flushing with He;
(B) $^{12}CH_3OH$ adsorption, followed by flushing with He and adsorption of $^{11}$C-methanol, all this at 333 K;
(C) $^{11}CH_3OCHO$ adsorption similarly to procedure A.

After the pre-adsorption procedures, the catalytic experiments were carried out under the conditions of step-wise temperature increase.

## 3. Results and discussion

### 3.1. Structural characterization

In Fig. 1 are presented nitrogen physisorption isotherms and pore size distribution (inset) for $ZrO_2$ support and selected copper modifications. The corresponding structural parameters are listed in Table 1. The isotherms are of IV type with a smooth step due to capillary condensation in the 0.6–1.0 relative pressure region and close to H1 hysteresis loop. According to IUPAC classification these features are typical of mesoporous materials with almost cylindrical pores (average pore diameter of 8 nm) [27]. The isotherms do not change in their shape after the modification which is evidence for the preservation of zirconia mesoporous structure even during the decomposition of copper precursor. A well defined tendency of specific surface area and pore size distribution decrease with copper loading increase is observed, which could be due to partial pore blocking. This effect is smallest for the sample with 4 wt.% Cu loading probably due to the predominant deposition of monolayer of finely dispersed copper species on the support. For comparison, SBA-15 silica possesses much higher BET surface area and pore volume, developed by uniform cylindrical mesopores with average pore diameter about 6 nm (Table 1). After the silica modification, the observed significant decrease in the pore volume and specific surface area clearly indicates pore blocking even at low (4 wt.%) copper loading, probably due to the predominant deposition of copper phase into the pores.

XRD patterns of all copper modifications are presented in Fig. 2. XRD pattern of $ZrO_2$ support represents reflections at 28.2° and 31.6° 2$\theta$, which are typical of monoclinic phase (space group P21/c) and the characteristic diffraction line at 30.6°, corresponding to tetragonal $ZrO_2$ (space group P42/nmc) with average crystalline size (calculated by Scherer equation) about 8 and 5 nm, respectively. The simultaneous presence of monoclinic and metastable tetragonal phase under ambient conditions was

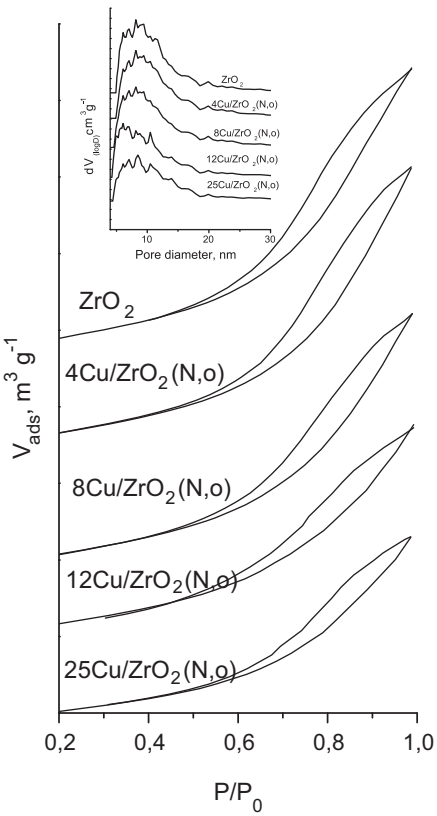


**Fig. 1.** Nitrogen physisorption isotherms and pore size distribution (inset) for $ZrO_2$ and various copper zirconia modifications.

previously described by Garvie [44] and Chraska et al. [45] as a result of particle size effect. For the small particles with a critical size about 9–30 nm the stability of tetragonal phase at room temperature was typically explained by the lower surface energy of tetragonal as compared to the monoclinic $ZrO_2$ phase. Li et al. [46] and Fabris et al. [47] proposed stabilization of metastable tetragonal and cubic phase by the formation of oxygen vacancies.

After the modification, a decrease in the portion of zirconia tetragonal phase is observed (Fig. 2, Table 1) and this could be related to a decrease in the number of oxygen vacancies in the zirconia lattice probably due to the capture of copper species on them [32,48 and refs therein]. No reflections of any copper containing phase are registered for both 4 wt.% copper modifications obtained from different copper precursors, while slight and not well resolved reflections at 35.2° and 38.5° $2\theta$ of tenorite CuO phase are detected for both 8 wt.% modifications. After the reduction, the appearance of very slight reflection at 43° $2\theta$ for these samples indicates presence of finely dispersed metallic copper particles. The reflections in the patterns of oxidized samples (Fig. 2) become more intensive with further copper loading increase corresponding to well crystallized CuO particles with average crystalline size of about 16–21 nm. The observed XRD and nitrogen physisorption results (see above) well correlate with the literature data [9,47,49] for the limit in the amount of copper that can be loaded on $ZrO_2$ before the appearance of crystalline CuO (about 4–5% per each 100 $m^2/g$ of $ZrO_2$ support). Besides, no reflections are observed for 4Cu/SBA-15(N,o). However, contrary to 8Cu/$ZrO_2$(N,o), well crystallized CuO with average crystalline size of about 40 nm is detected for 8Cu/SBA-15(N,o). Taking into account the higher BET surface area and pore volume for SBA-15 in comparison with mesoporous $ZrO_2$ (Table 1), the decisive role of copper/support interaction over the effect of textural characteristics of the support could be assumed.

### 3.2. Spectroscopic data

UV–vis spectroscopy is a powerful method to obtain information for the coordination and different oxidation state of metal ions by measuring d–d and f–d transitions and oxygen–metal ion charge transfer bands. According to [50–53] the observed main absorption band at 228 nm and the broad shoulder above 275 nm in the spectrum of pure $ZrO_2$ support (Fig. 3) could be assigned to inter-band and low-coordinated surface $Zr^{4+} \leftarrow O^{2-}$ transitions, respectively, in monoclinic and tetragonal $ZrO_2$. This is in a good correlation with the XRD data, where a mixture of both phases was observed (Fig. 2). The spectra of all zirconia copper modifications represent intensive absorption features in 300–500 nm region and above 720 nm which could be assigned to CT and d–d- transitions in oligomeric Cu–O–Cu species and well crystallized CuO particles, respectively [54,55]. For comparison, the silica analogues exhibit intensive absorption features at about 250 nm and above 740 nm, typical of $Cu^{2+} \leftarrow O^{2-}$ CT and d–d transitions in crystalline CuO. The observed differences in

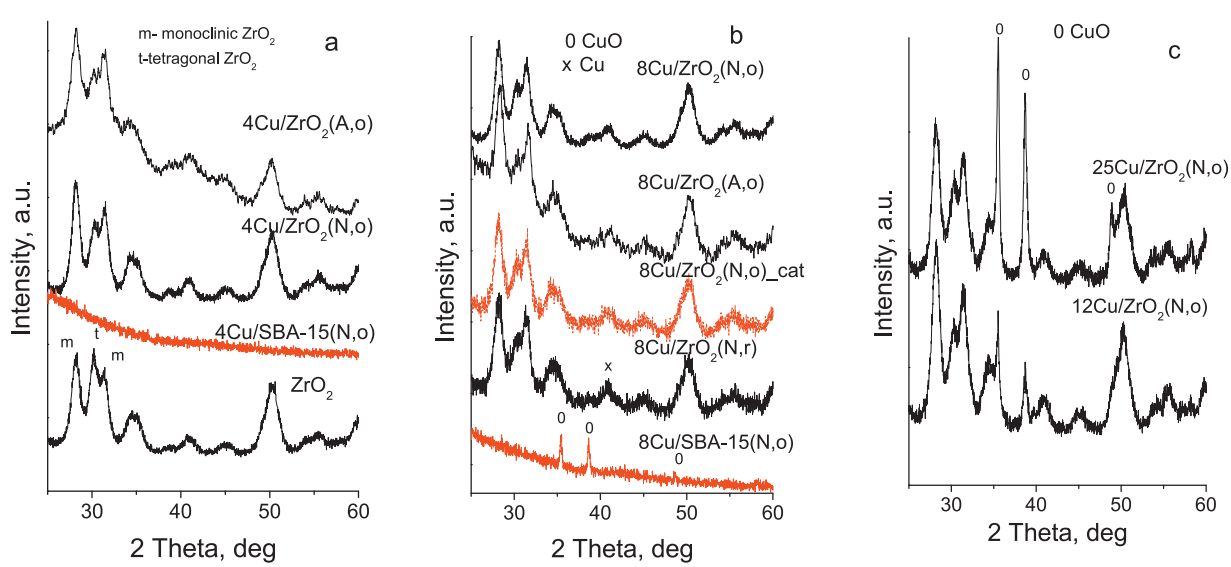


**Fig. 2.** XRD patterns of pure $ZrO_2$ and various copper modifications of $ZrO_2$ and SBA-15 silica obtained by nitrate (N) or acetyl acetonate (A) precursors. For comparison, XRD patterns after reduction (r) and catalytic test (cat) for 8Cu/$ZrO_2$ (N,o) are also presented in (b).

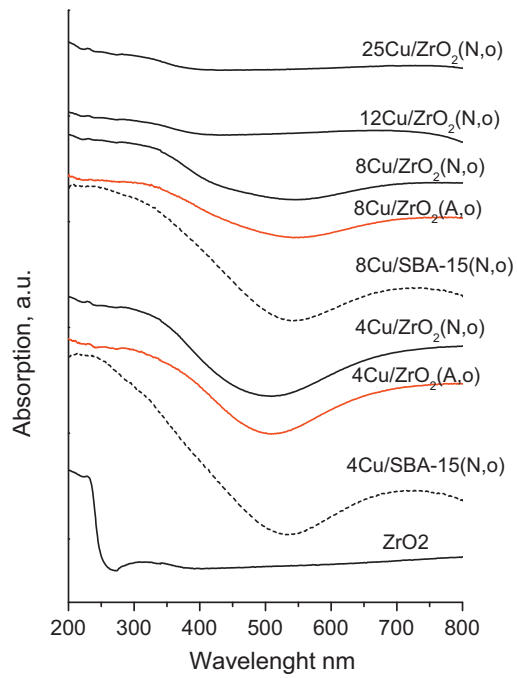


**Fig. 3.** UV–vis spectra of copper modifications of $ZrO_2$. For comparison, the spectra of selected copper modified SBA-15 are also presented (dash lines).

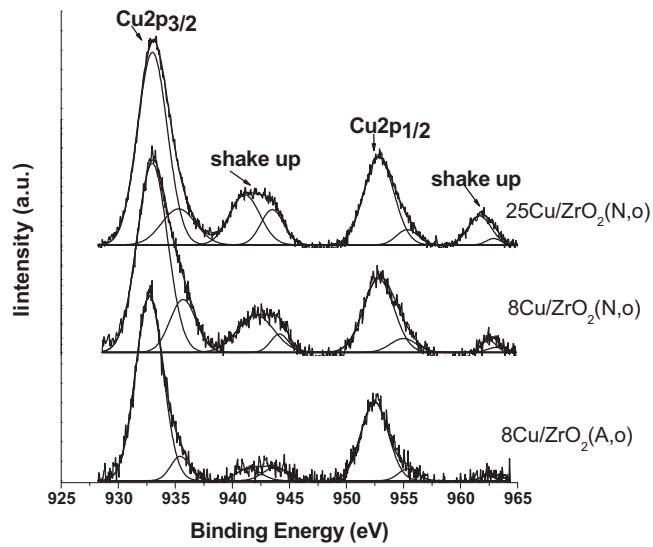


**Fig. 4.** Cu 2p photoelectron spectra of selected samples.

the UV–vis spectra of silica and $ZrO_2$ based modifications could be due to the presence of more finely dispersed copper species on zirconia support, which is also in agreement with the XRD data (see above).

The FTIR spectrum of pure $ZrO_2$ (Supporting information, Fig. S1) consists of broad bands at approximately 420, 504, 590 and 750 $cm^{-1}$ which is due to Zr–O stretching vibrations in $ZrO_x$ polyhedron with typical values of $x = 4$ or 6 for monoclinic phase [56]. The similarities in the FTIR spectra of pure and modified $ZrO_2$ is not surprising, since in general, all polymorphs are very similar in vibration structure [56]. However the observed minor variations in the band frequencies and intensities after the modification could be carefully assigned to small differences in $Zr^{4+}$ distribution in $ZrO_x$ sites and oxygen vacancies. In accordance with the XRD data, these observations for the modified samples could be due to lowering symmetry of the structure as a result of tetragonal to monoclinic $ZrO_2$ phase transitions. The Cu–O stretching modes, which generally appear at 515, 480 and 450 $cm^{-1}$, could not be clearly resolved due to their superposition with the modes of $ZrO_2$ support [57].

Cu $2p_{3/2}$ and Cu $2p_{1/2}$ XP core level spectra of selected zirconia modifications are shown in Fig. 4 and the corresponding XP parameters are summarized in Table 2. As shown in Fig. 4 the main Cu 2p spin orbit components, Cu $2p_{3/2}$ and Cu$2p_{1/2}$, are accompanied with shake up peaks located at about 9 eV higher binding energy (BE) with respect to the main peaks. The presence of such satellites is typical of $Cu^{2+}$ species [58]. From the curve fitting, the binding energies of the two Cu $2p_{3/2}$ components reported in Table 2 are obtained. The position of the first peak is at 932.7–933.1 eV, while the second one is typically situated at 935.2–935.4 eV BE. The low energy peak could be related to CuO although, the observed Cu $2p_{3/2}$ BEs for all samples were lower (Table 2) than the reported one for pure CuO (933.5 eV) [58,59]. The high energy peak can be assigned to $Cu(OH)_2$, also characterized by shake up satellites [59]. The experimental ratio between the overall intensity of the satellite peak ($I_{sat}$) with respect to the overall intensity of the main peak ($I_m$) is between 0.10 and 0.38 (Table 2), which is below the one reported for bulk CuO [58,59]. Similar decrease in the $I_{sat}/I_m$ ratio has been previously observed for copper modified ZnO, particularly for materials with low Cu/Zn ratio [60], and it was attributed to the dissolution of $Cu^{2+}$ species in ZnO. Alternatively, Moretti et al. [61] assigned this phenomenon to the existence of a strong interaction between CuO and ZnO, leading to a more covalent Cu–O bond. Here, the observed $I_{sat}/I_m$ ratio, along with the lower Cu $2p_{3/2}$ BEs, indicates that CuO and $ZrO_2$ are not simply physically mixed in the $CuO/ZrO_2$ catalysts but an interaction between them exists. This assumption is also supported by the observed lower values of Zr $3d_{5/2}$ BE for all copper modifications (Table 2) as compared to the BE reported for the prepared by different techniques mesoporous $ZrO_2$ (183.1 eV) [62]. Note, the absence of any significant effect of samples composition on the Zr $3d_{5/2}$ BE with copper loading increase above 8 wt.%. However, for the samples $8Cu/ZrO_2$(A,o) and $8Cu/ZrO_2$(N,o) smaller Cu/Zr ratios are observed, which clearly indicates surface copper depletion (Table 2). Quite interesting, with the decrease of the copper loading a decrease of the shake up peak with respect to the primary photoelectron peak is observed ($I_{sat}/I_m$) particularly in the sample from the acetyl acetonate precursor. Such decrease is in accordance with the presence of Cu or $Cu_2O$. Indeed, with respect to their Cu $2p_{3/2}$ binding energies which are slightly lower than the $Cu^{2+}$ ones, about 932.6 eV for CuO and 932.4 eV for $Cu_2O$ [63], the absence of the shake up satellites is generally better indication of their presence. Moreover the peaks related to Cu and $Cu_2O$ cannot be resolved by deconvolution because their BEs are very close (differ only by 0.1 eV) [63]. Therefore the Cu $L_3M_{4,5}M_{4,5}$ Auger spectra and the calculated modified Auger parameter ($\alpha'$) were used to determine the chemical state of copper in these samples (Table 2). The samples with relatively low copper loading, $8Cu/ZrO_2$(N,o) and $8Cu/ZrO_2$(A,o), possess lower values of both Cu $L_3M_{4,5}M_{4,5}$ kinetic energy (KE) and $\alpha'$ than the samples with relatively high copper loading, $12Cu/ZrO_2$(N,o) and $25Cu/ZrO_2$(N,o). The difference in the above sets of values clearly points to the formation of $Cu_2O$ facilitated at low copper loading, to a higher extent when copper acetyl acetonate precursor is used, while increase in CuO portion is found with copper loading increase.

So, the obtained XPS and XRD data urge the authors to assume that at low copper loading (below 8 wt.%) formation of copper oxide monolayer on mesoporous $ZrO_2$ occurs, while well crystallized CuO phase forms over this monolayer with the copper loading increase. The close contact between CuO and $ZrO_2$ nanoparticles results in intensive electron transfer between zirconia support and copper particles which facilitates stabilization of $Cu^+$ species in the

**Table 2**
XPS binding energies of the sample element main peaks and kinetic energy of the Auger CuLMM. The modified Auger parameter has been calculated as the $Cu2p_{3/2}$ binding energy minus the Auger kinetic energy plus the X-ray photon energy (Al $K_\alpha$ = 1486.6 eV).

| Sample | Cu $2p_{3/2}$ (eV) | $I_{sat}/I_m$ | Cu $L_3M_{4,5}M_{4,5}$ (eV) | $\alpha$ (eV) | $Zr3d_{5/2}$ (eV) | Cu/Zr | O1s |
|---|---|---|---|---|---|---|---|
| $ZrO_2$ | | | | | 183.1 | | 530.6(92)<br>532.8(08) |
| 8Cu/$ZrO_2$(N,o) | 932.9<br>935.4 | 0.24 | 915.4 | 1848.3 | 182.5 | 0.14 | 530.2(87)<br>532.3(13) |
| 8Cu/$ZrO_2$(A,o) | 932.7<br>935.3 | 0.11 | 915.3 | 1848.0 | 182.6 | 0.09 | 530.2(87)<br>532.2(13) |
| 12Cu/$ZrO_2$(N,o) | 933.0<br>935.2 | 0.33 | 917.7 | 1850.7 | 182.4 | 0.27 | 530.1(93)<br>532.7(07) |
| 25Cu/ZrO2(N,o) | 933.1<br>935.4 | 0.38 | 918.0 | 1851.1 | 182.5 | 0.36 | 530.2(90)<br>532.4(10) |

interface monolayer. This effect is more pronounced when copper acetyl acetonate was used, and probably originates with different mode of interaction of the precursor with surface functionality [40,41]. Easier reduction of loaded copper species by the products of acetyl acetonate decomposition is suggested, and we'll return to this point during the TPR study.

### 3.3. Temperature programmed reduction

More information for the state of copper species was obtained by temperature programmed reduction (TPR) with hydrogen (Fig. 5, Table 3). Principally, this method could be very informative for the oxidative state and environment of metal ions, but usually the interpretation of the obtained results is rather complicated due to the superposition of various effects, originating from variations in particle size and interaction of metal ions with the support. Besides, Soczyski et al. [64], studying the reduction kinetics of CuO in CuO/ZnO/$ZrO_2$ systems, found that the reduction of CuO is a consecutive autocatalytic reaction. This autocatalytic effect is due to facilitated dissociation of $H_2$ on the metallic copper formed [64], which additionally renders difficult the interpretation of TPR results. The facilitated role of $ZrO_2$ support on the reduction of loaded copper oxide particles is well established phenomenon, but there are some controversial explanations of the observed TPR effects. Liu et al. [65] reported two overlapping TPR features during the reduction of CuO supported on tetragonal $ZrO_2$ which was explained with step wise reduction ($Cu^{2+} \rightarrow Cu^{+} \rightarrow Cu^{0}$) of highly dispersed CuO particles. Zhou et al. [66] also reported presence of two reduction peaks at relatively low temperature, one centered around 450 K ($\alpha$ peak) and second one, around 468 K ($\beta$ peak), both of them attributed to the reduction of highly dispersed copper species [65]. The appearance of third peak ($\gamma$ peak) for the samples with higher copper content has been assigned to the reduction of bulk CuO particles [65]. The latter peak could be broader and shifted toward higher temperatures when Cu content increased [67]. Contrary, Aguila et al. [68] reported strong interaction in low loaded CuO/$ZrO_2$ materials which results in reduction effect above 573 K. Ma et al. [19] observed significant differences during the reduction of CuO particles on amorphous, monoclinic and tetragonal $ZrO_2$ and they assigned this phenomenon to different surface properties of zirconia supports. They proposed that the intimate contact between CuO and $ZrO_2$ results in activation of $H_2$ molecule on oxygen vacancies on $ZrO_2$ surface, which facilitates the reduction process. Zhao et al. [69] explained different TPR profiles for copper modified monoclinic and tetragonal zirconia as a result of different degree of coordination of lattice $O^{2-}$ ions in monoclinic (3- and 4- coordinated) and tetragonal (4-coordinated) $ZrO_2$ lattice, which provides different interaction between $Cu^{2+}$ and $O^{2-}$. In our study, the comparison of TPR profiles for analogues copper modifications, supported on $ZrO_2$ and SBA-15 (Fig. 5, Table 3) confirm existence of copper-support interaction in the former materials. As compared to the silica samples, the reduction of $ZrO_2$ modifications starts at about 50–100 K lower temperature. Moreover, the reduction profiles are complex and consist of several overlapping effects. The low-temperature $\alpha$ and $\beta$ effects appear for all nitrate Cu/$ZrO_2$ modifications. The preservation of the relative part of these effects with copper loading increase indicates that they probably originate from the reduction of CuO particles in interface monolayer, which interacts with monoclinic and tetragonal $ZrO_2$ phase, even though we can not fully exclude a step-wise reduction of finely dispersed CuO particles in this layer. Note that the TPR profiles for copper modifications obtained by acetyl acetonate precursor consist of only one narrow low-temperature effect. This confirms different mode of interaction of acetyl acetonate precursor with surface functionality, according to [40,41] which provides the formation of more uniform Cu-species. Taking into account XPS results, this observation can be also assigned to the predominant reduction of $Cu^{+}$ ions. A high temperature effect ($\gamma$) situated at about 500 K also appears for the samples with higher copper loading. The comparison with the silica analogues clearly indicates that it is due to the reduction of bulk CuO phase (Fig. 5, Table 3). We would like also to stress on the much higher weight loss for all zirconia modifications than the expected theoretic one for the reduction of loaded CuO. In order to clear this effect, the hydrogen consumption during the TPR experiments was measured for selected samples (Supporting information, Fig. S2). The absence of any hydrogen consumption peak (not shown) in TPR profile of pure zirconia indicates that the observed weight loss in the TPR-TG profiles (Fig. 5, Table 3) is only related to the release of surface hydroxyl groups. At the same time, the appearance of several sharp peaks between 323 K and 573 K and a broad peak from 573 K to 1073 K is registered for the copper modification (4Cu/$ZrO_2$(N,o). Quantitative analysis for the low temperature (6.6 $\mu$mol of $H_2$) and high temperature (5.8 $\mu$mol of $H_2$) effects evidences reduction of the loaded copper phase and $H_2O$ evolution, respectively. We assign the latter feature to the release of surface OH-groups, which are continually restored *via* spillover of hydrogen from copper to zirconia, as was described in [70]. Moreover, the low-temperature weight loss corresponds to about 75% reduction of $Cu^{2+}$ to metallic copper, which clearly confirms the data from XPS analyses for the formation of $Cu^{+}$ on zirconia support. For comparison, the reduction degree for all silica supported materials is below the theoretical one (Table 3), which indicates presence of isolated ions or finely dispersed species in strong interaction with the surface silanol groups.

### 3.4. Methanol decomposition catalytic test

In Fig. 6 are presented data for methanol conversion on copper modified $ZrO_2$ materials at 500–770 K under temperature programmed regime. The selectivity to CO, which pursues the main reaction pathway for hydrogen production from methanol, is shown as most representative. Pure $ZrO_2$ exhibits relatively low

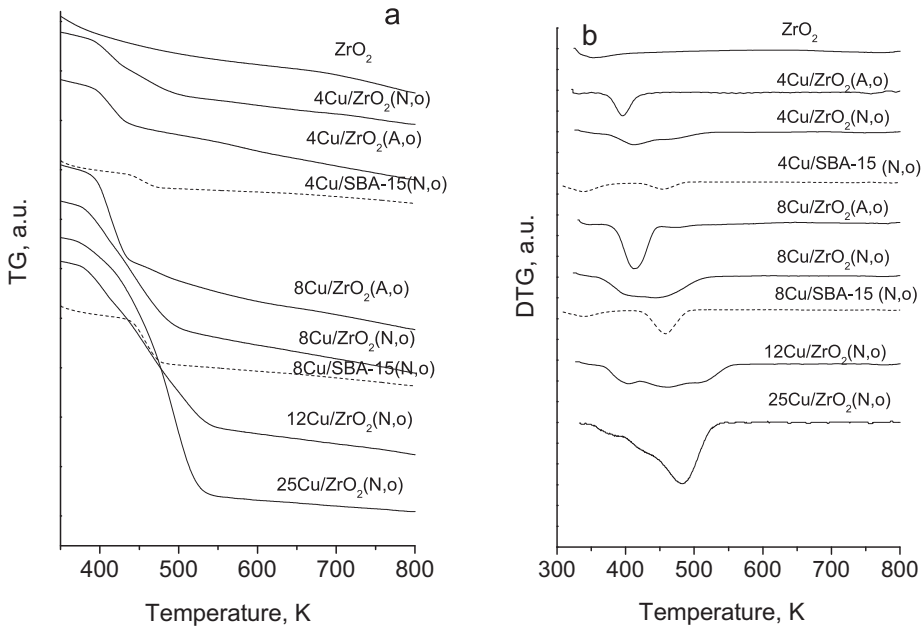


**Fig. 5.** TPR-TG (left) and TPR-DTG (right) profiles of pure $ZrO_2$ and its copper modifications. For comparison, selected TPR profiles of SBA-15 silica based modifications are also shown.

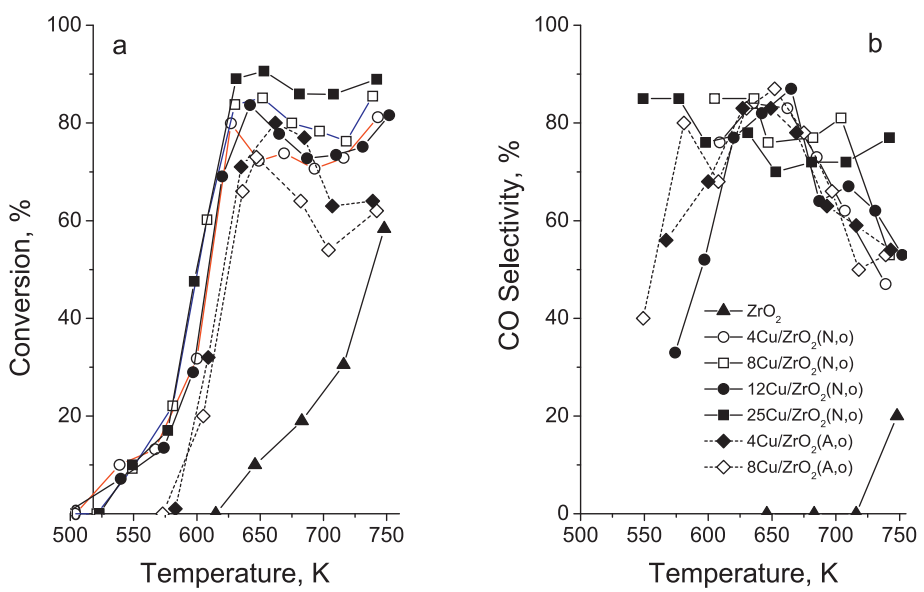


**Fig. 6.** Methanol conversion (a) and CO selectivity (b) vs. temperature for all copper zirconia materials.

**Table 3**
Initial reduction temperature (*T* ini), temperature of reduction maximum (*T* max), experimental (at 350–750 K region) and theoretic weight loss (CuO → Cu) during TPR with hydrogen of copper modifications.

| Sample | $T_{ini}$, K | $T_{max}$, K | Theoretic weight loss, mg | Experimental weight loss, mg |
|---|---|---|---|---|
| $ZrO_2$ | | | 2.6 | 0.42 |
| 4Cu/$ZrO_2$(N,o) | 372 | 411,465 | 0.40 | 0.83 |
| 4Cu/$ZrO_2$(A,o) | 362 | 394 | 0.40 | 0.77 |
| 8Cu/$ZrO_2$(N,o) | 357 | 417,450 | 0.80 | 1.70 |
| 8Cu/$ZrO_2$(A,o) | 372 | 412 | 0.80 | 1.64 |
| 12Cu/$ZrO_2$(N,o) | 353 | 400,460,520 | 1.21 | 1.92 |
| 25Cu/$ZrO_2$(N,o) | 345 | 376,420,480 | 2.52 | 2.71 |
| 4Cu/SBA-15(N,o) | 411 | 452 | 0.40 | 0.28 |
| 8Cu/SBA-15(N,o) | 421 | 456 | 0.80 | 0.72 |

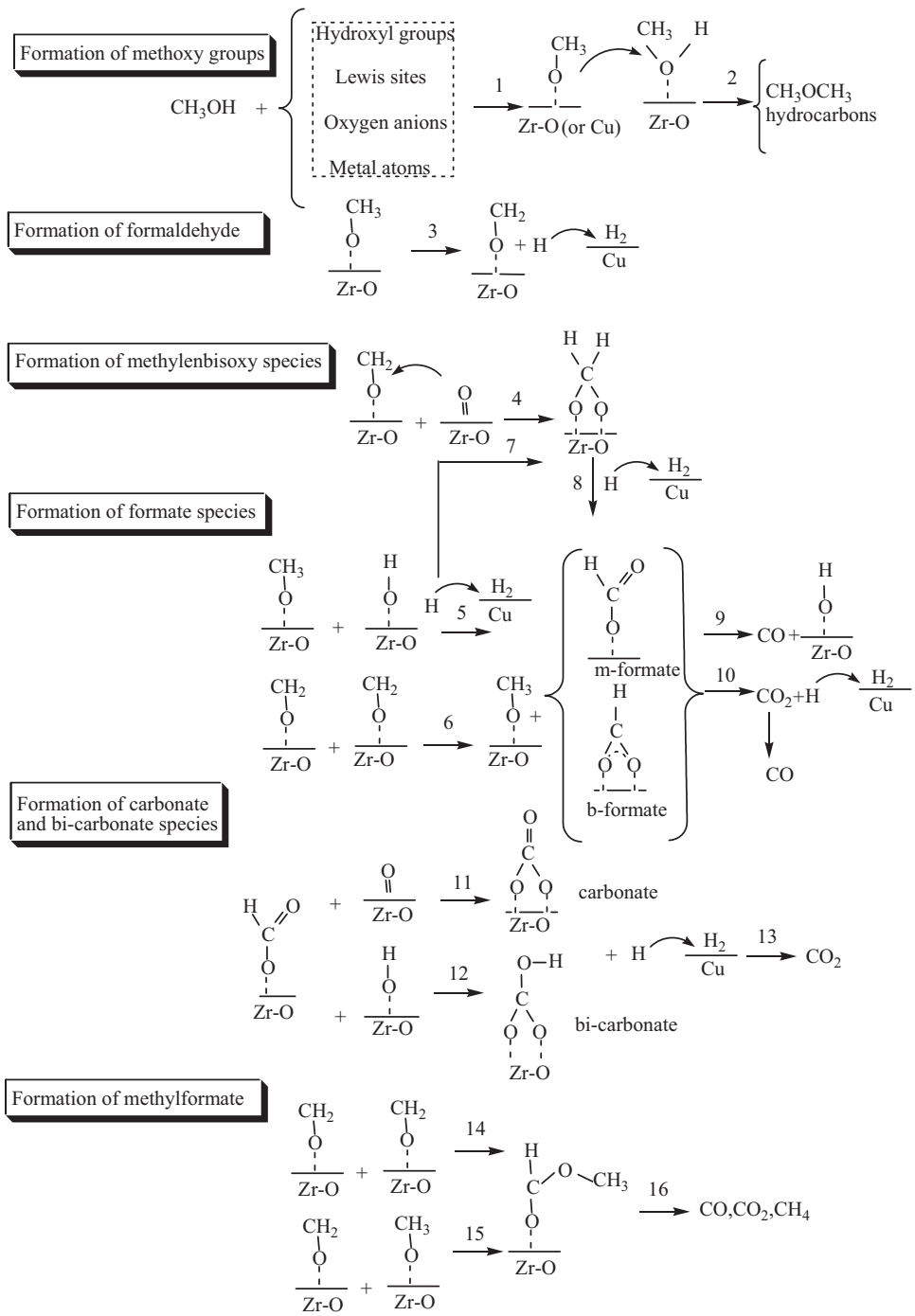


**Scheme 1.** Possible pathways of methanol conversion on zirconia catalysts.

ability for methanol decomposition to CO and $H_2$ even above 600 K. Here, maximum conversion of 60% and about 20% selectivity to CO are observed at 770 K. The main by-product (up to 90%) from the conversion is dimethyl ether (DME), which is related to the acidic function of the support. The acidic nature of $ZrO_2$ was clearly confirmed also by the spectrum of adsorbed pyridine (Supporting information, Fig. S3), that shows two main adsorption peaks at 1445 and 1607 $cm^{-1}$, which are resistant to the outgassing up to 523 K [71,72]. Small amount of $CO_2$ (up to 12%) and methane (up to 10%) are also registered during the methanol decomposition on pure $ZrO_2$ support. The modification of $ZrO_2$ with copper strongly increases the catalytic activity which is evident from the about 100 K low temperature shift of the conversion curves (Fig. 6a). Further, a significant increase in CO selectivity to the expense of DME decrease is observed (Fig. 6b). A common feature for all materials is the complex course of the conversion curves (Fig. 6a), all of them with a maximum at about 640 K and a tendency of conversion increase above 690–700 K. Note, that this catalytic behavior is observed even for $4Cu/ZrO_2$(N,o) and it was not affected significantly from the further copper loading increase. A possible reason for the observed effect could be the agglomeration of copper particles during the catalytic test, but this was not confirmed by the XRD study of the used in the catalytic test catalysts (selected pattern is presented in Fig. 2). No significant changes with the zirconia support after the catalytic test were registered as well. On the base of XRD, nitrogen physisorption and TPR data (see above),

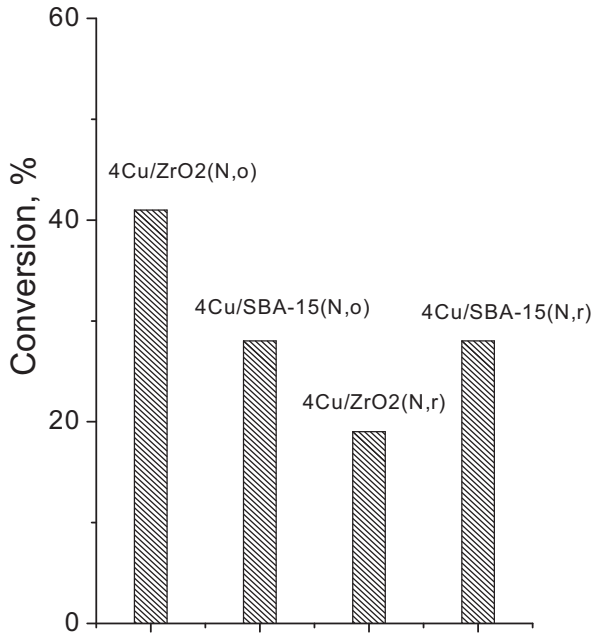


**Fig. 7.** Methanol conversion at 600 K for 4Cu/$ZrO_2$ and 4Cu/SBA-15 after samples pre-treatment in oxidative (o) and reduction (r) atmosphere.

we could assume that the catalytic behavior of Cu/$ZrO_2$ modifications originates predominantly from the copper-zirconium oxides interface layer and it is slightly influenced by the presence of bulk CuO species. Size-dependent effect of supported on ZnO and $CeO_2$ copper oxide nanoparticles during the oxidative steam reforming of methanol was reported also in [35,73]. In order to prove this assumption, the catalytic activity of 4Cu/$ZrO_2$(N,o) with its silica based analogue were compared (Fig. 7, Supporting information, Fig. S4). We would like to remind (see above) that for this sample the formation of monolayer of CuO over zirconia support was predominantly assumed. The complex course of conversion curves, which is detected for zirconia modification, is not typical for the SBA-15 based catalysts (Supporting information, Fig. S4). The presented histograms (Fig. 7) clearly show that $ZrO_2$ facilitates the catalytic activity of loaded CuO, but contrary to the silica modification, the preliminary reduction of Cu/$ZrO_2$ decreases the conversion. Some authors [48] considered the decisive role of oxygen vacancies on $ZrO_2$ surface which contribute to the formation of active sites *via* capture of copper species. In this way, zirconia could improve not only the dispersion of copper oxide particles, but also the electron exchange in the catalytically active $Cu^{2+}$-$Cu^{+}$ or $Cu^{+}$-$Cu^{0}$ pairs. This could provide facile splitting of O–H bond in the adsorbed methanol molecule with the formation of surface methoxy species which further transform to other carbon-containing intermediates, according to Scheme 1. The reduction medium, which also exists during the methanol decomposition, could easily decrease the number of these redox pairs at relatively low temperature (see XRD data) with the formation of new type of metallic copper catalytic sites. As a result, changes in the mechanism of methanol decomposition at higher reaction temperature are expected. Taking into account that the methanol adsorption ability over metallic copper is very low [74], the contribution of these copper particles could be mainly in the hydrogen release [75], while the formation of various intermediate species predominantly occurs on the zirconia surface (Scheme 1). Thus, the observed complex changes in the conversion curves (Fig. 6a) could be due to different mode of synergistic activity in copper-zirconia bi-component system and this is controlled by the reduction changes with copper species under the reaction medium. Similar effect of changes in the reaction pathways with the reduction of copper phase by the reaction medium during the oxidative steam reforming of methanol on Cu/ZnO was discussed in [35,36]. Obviously, the synergistic effect depends on the state of copper species and their environment and this is confirmed with the observed lower catalytic activity for acetyl acetonate obtained materials, where according to XPS and TPR data, formation of uniform copper, but predominantly $Cu^{+}$ species is observed (Fig. 6a).

### *3.5. Catalytic experiments with $^{11}$C-labeled methanol and $^{11}$C-methyl formate*

In order to obtain more information for the primary products of methanol conversion on copper modified zirconia and the role of different catalytic sites during the reaction, catalytic experiments with low and selective coverage of the surface with radio labeled $^{11}CH_3OH$ are performed. Two different procedures for adsorption of methanol before the catalytic experiments were applied. The procedure (A) includes $^{11}CH_3OH$ adsorption at 333 K, followed by heating up to 373 K and flushing of the released methanol with He. Under these conditions, very low coverage of the surface with predominant occupation of the strongest adsorption sites with $^{11}CH_3OH$ is expected. Alternatively, the sample was also studied after procedure (B), where before the adsorption of $^{11}CH_3OH$ at 333 K, the surface was partially covered with $^{12}CH_3OH$ at the same temperature. In this way, the $^{11}CH_3OH$ molecules situate predominantly only on the weakest adsorption sites, while the stronger one are occupied by $^{12}CH_3OH$. For the pure $ZrO_2$ support (Fig. 8a, b) no products of methanol conversion are registered at 473 K, while propene was detected as a primary product at 523 K (Fig. 8a, curve 1). Taking into account that the formation of olefins from methanol is typical for strong Broensted acidic sites [76,77], the observed results evidence their presence on the $ZrO_2$ support. Some authors also discuss the existence of strong Broensted sites (mainly in monoclinic $ZrO_2$), which could be formed by the influence of oxygen vacancies in the vicinity of Zr–OH groups [13]. According to the proposed in [78] "carbon pool mechanism", the formation of propene occurs from surface methoxy groups on zirconia (Scheme 1, routes 1, 2). DME appears with the temperature increase up to 573 K, which is an indication for the activity of additional weaker acidic sites (Broensted and/or Lewis). Besides, $CO_2$ is also detected (Fig. 8a, curve 2) under these conditions. This could be provoked by a consecutive transformation of surface methoxy groups [75] to methylenbisoxy ones [79] and then to formate species according to (Scheme 1, routes 5–8) [80]. Alternatively, $CO_2$ can be produced *via* decomposition of surface carbonate and bi-carbonate groups (Scheme 1, routes 11 and 12 respectively) [19], or *via* decomposition of surface methyl formate species [75] (Scheme 1, route 14). Further temperature increase results in almost complete conversion of methanol to a mixture of CO and $CO_2$ (Fig. 8a, curve 3). The appearance of CO among the products could be due to the decomposition of formate species with the recovery of surface OH groups (Scheme 1, route 9) or due to decomposition of methylformate (Scheme 1, route 16) [80]. Some differences in methanol conversion occur after the procedure B, where the stronger sites are blocked by $^{12}CH_3OH$ and only the weakest ones are engaged with $^{11}CH_3OH$ (Fig. 8b). Here again, the acidic function of $ZrO_2$ is well manifested, but very low degree of methanol decomposition to CO and $CO_2$ even at 623 K is observed. Obviously the weaker sites contribute to the formation of surface methoxy groups, which further transform predominantly to DME and hydrocarbons (Scheme 1, routes 1, 2) and convert in much less extent to formate intermediates.

Copper modification provides formation of DME at significantly lower temperature as compared to $ZrO_2$ support when it is covered with $^{11}$C-methanol following the procedure (A) (Fig. 8d, curve 1). This could be related to the formation of additional acidic sites

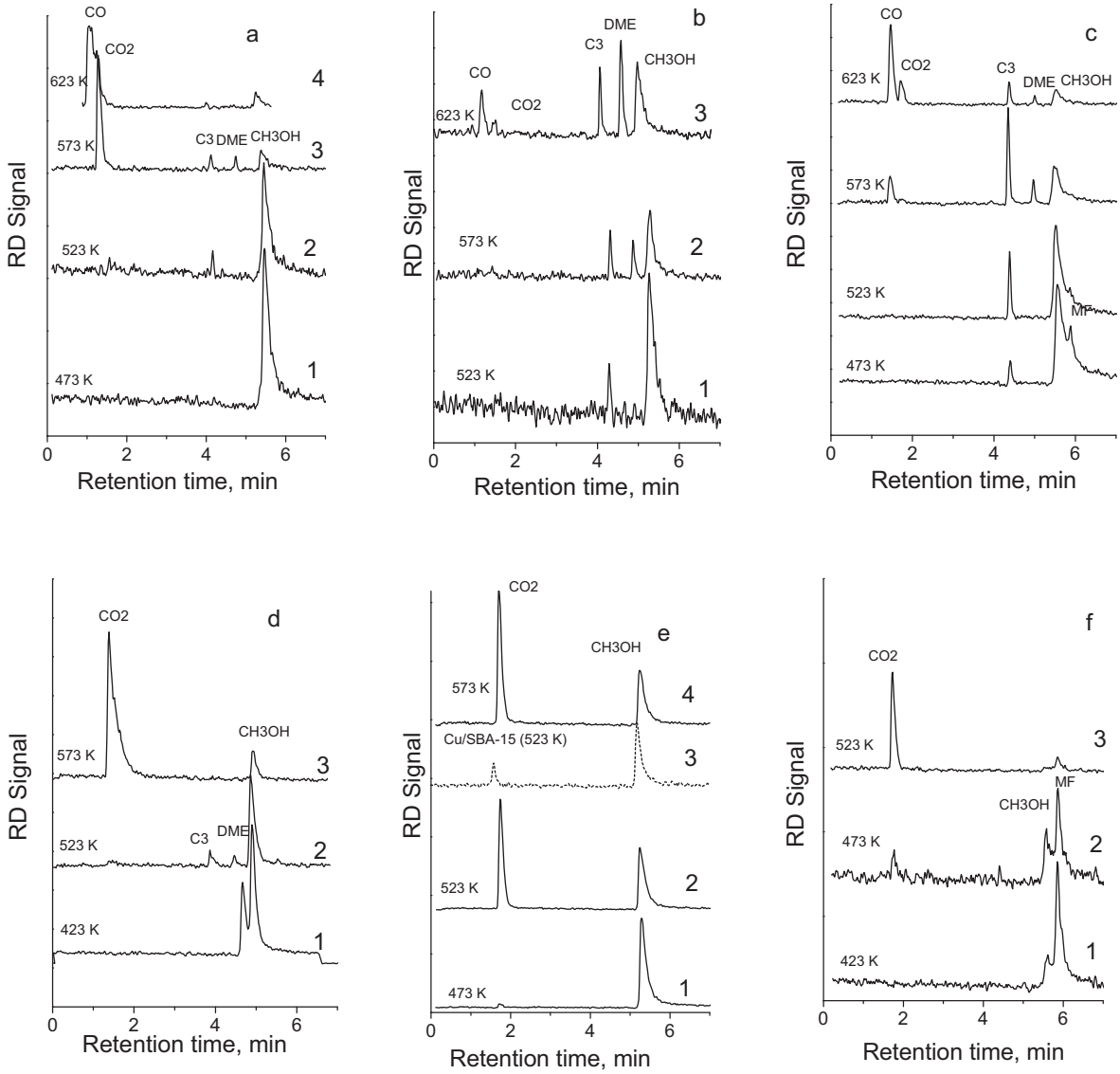


**Fig. 8.** $^{11}CH_3OH$ decomposition at various temperatures on: $ZrO_2$ after procedure A (a), $ZrO_2$ after procedure B (b), $8Cu/ZrO_2$(N,o) after procedure A (d) and $8Cu/ZrO_2$(N,o) after procedure B (e). $^{11}CH_3O$-CHO decomposition after procedure C on $ZrO_2$ (c) and $8Cu/ZrO_2$(N,o)(f).

and this is clearly confirmed by the broadening of the two bands corresponding to the Lewis sites in the spectra of adsorbed pyridine of dehydrated 4 wt.% $CuO/ZrO_2$ in comparison with pure $ZrO_2$ (Supporting information, Fig. S3). According to [81,82] this can be ascribed to the presence of coordinative unsaturated copper sites in small metal oxide nanoparticles. Moreover, the heating leads to an increase and a shift of the band at 1487 $cm^{-1}$ (Supporting information, Fig. S3) that is usually assigned to pyridine lying on both Lewis and Brönsted sites. The formation of a broad band around 1540 $cm^{-1}$ and of a shoulder (at around 1620 $cm^{-1}$) of the band at 1612 $cm^{-1}$ confirm the formation of Brönsted sites [71,72]. These assumptions are also confirmed by the spectra of reduced $4Cu/ZrO_2$(N,r) material (Supporting information, Fig. S3) where similar features, but with lower intensity are observed due to higher dehydroxylation under the reduction conditions [81–83]. The observed higher ability to $CO_2$ formation for $Cu/ZrO_2$ as compared to the pure $ZrO_2$ support indicates the increase in the redox function probably due to the increased dispersion of copper particles and synergistic effect with $ZrO_2$ support, as was discussed in the previous section. Note that after the procedure B the acidic function is fully suppressed and $CO_2$ is the only registered product above 473 K (Fig. 8e, curves 2, 3). Under these conditions the catalytic behavior of both $ZrO_2$ and silica copper modifications is very similar, but lower catalytic activity for the latter is observed (Fig. 8e, dash line). This confirms again that copper and zirconia behave in a synergistic manner, which results in higher dehydrogenation ability even on weakly adsorbing sites. It seems that in this case $CO_2$ is produced mainly from the decomposition of formate intermediates on highly dispersed copper species (Scheme 1, routes 3, 6). This confirms our assumption that the mechanism of methanol decomposition on $Cu/ZrO_2$ depends on the experimental conditions. Predominant participation of $Cu^{2+}$-$Cu^{+}$ or $Cu^{+}$-$Cu^{0}$ pairs is expected under milder conditions (lower temperatures) with the activity of weakly adsorbed sites or in bi-functional manner at more steady conditions with the participation of strongly adsorbed sites. Besides, nowadays the participation of methyl formate as intermediate in methanol decomposition is a matter of controversial discussion [84]. Some researchers who detected methyl formate proposed that it was formed by dimmerization of formaldehyde molecules according to Tischenko mechanism (Scheme 1, route 14) [85], while Takahashi et al. [86] and Lin et al. [87] proposed that methyl formate was formed by the reaction between methoxy

and formaldehyde involving hemiacetal-like species (Scheme 1, route 15). In our study we didn't find MF among the primary products of methanol decomposition. Fisher and Bell [75] also do not observed MF in the gas products during the conversion of methanol on $Cu/ZrO_2$ and related this phenomenon to its stabilization on the surface. In order to obtain more information, we investigated the decomposition of $^{11}CH_3OCHO$ (procedure C, Fig. 8c and f). The formation of labeled methanol, propene and DME at relatively low temperatures on pure $ZrO_2$ support (Fig. 8c) evidences that MF decomposes with the formation of $^{11}CH_3OH$, which further transforms on surface acidic sites according to Scheme 1, route 2. The observed higher selectivity to CO in comparison with the experiments starting with $^{11}C$-methanol (Fig. 8a) urged the authors to assume that MF is not mandatory intermediate during the methanol conversion on $ZrO_2$. This assumption is valid also for the $Cu/ZrO_2$ sample, where much higher activity and selectivity to $^{11}CO_2$ is observed when $^{11}CH_3OCHO$ is used as a reactant (Fig. 8f) as compared to the experiments starting from $^{11}C$-methanol (Fig. 8d).

## 4. Conclusion

At lower copper loading (about 4 wt.%) formation of CuO monolayer on mesoporous $ZrO_2$ occurs, while well crystallized CuO phase forms over this monolayer with copper loading increase. The results from various physicochemical techniques and catalytic tests with selective coverage of catalysts with $^{11}C$-methanol or $^{11}C$-methylformate indicate that the synergistic effect in copper-zirconia interface monolayer realizes *via* (i) facilitate electron exchange in the copper ion pairs by improved dispersion and stabilization of $Cu^+$ ions on zirconia support, (ii) creation of additional acidic sites, which contribute to the formation of surface methoxy groups or (iii) in bi-functional manner, where $ZrO_2$ behaves as a reservoir of surface intermediates, which convert with spillover of hydrogen to metallic copper. It was established that MF is not mandatory intermediate during the methanol conversion on $ZrO_2$ and $Cu/ZrO_2$.


## Acknowledgments

Financial support BAS, Bulgarian National Science Fund at the Ministry of Education and Science under Project DFNI-E01/7/2012 and CNR, Italy-BAS, Bulgaria bilateral project are gratefully acknowledged.


## Appendix A. Supplementary data

## References


[1] A.B.F. Martinson, J.W. Elam, J.T. Hupp, M.J. Pellin, Nano Lett. 7 (2007) 2183–2187.
[2] A.G. Sato, D.P. Volanti, I.C. de Freitas, E. Longo, J.M.C. Bueno, Catal. Commun. 26 (2012) 122–126.
[3] A.M. Ruppert, K. Weinberg, R. Palkovits, Ang. Chemie. Int. Edit. 51 (2012) 2564–2601.
[4] J. Sun, K. Zhu, F. Gao, C. Wang, J. Liu, C.H.F. Peden, Y. Wang, JACS 133 (2011) 1096–11099.
[5] T. Tsuchida, J. Kubo, T. Yoshioka, S. Sakuma, T. Takeguchi, W. Ueda, J. Catal. 259 (2008) 183–189.
[6] M.M. Rashad, H.M. Baioum, J. Mat. Process. Technol. 195 (2008) 178–185.
[7] A. Behbahani, S. Rowshanzamir, A. Esmaeilifar, Proc. Eng. 42 (2012) 908–917.
[8] R.A. Espinoza-González, D.E. Diaz-Droguett, J.I. Avil, C.A. Gonzalez-Fuentes, V.M. Fuenzalid, Mater. Lett. 65 (2011) 2121–2123.
[9] K.V.R. Chary, K.K. Seela, D. Naresh, P. Ramakanth, Catal. Commun. 9 (2008) 75–81.
[10] D.P. Volanti, A.G. Sato, M.O. Orlandi, J.M.C. Bueno, E. Longo, J. Andrés, ChemCatChem 3 (2011) 839–843.
[11] K. Inui, T. Kurabayashi, S. Sato, J. Catal. 212 (2002) 207–215.
[12] J. Liu, J. Shi, D. He, Q. Zhang, X. Wu, Y. Liang, Q. Zhu, Appl. Catal. A 218 (2001) 113.
[13] M.D. Rhodes, K.A. Pokrovski, A.T. Bell, J. Catal. 233 (2005) 210.
[14] L. Wang, W. Zhu, D. Zheng, X. Yu, J. Cui, M. Jia, W. Zhang, Z. Wang, React. Kinet. Mech. Catal. 101 (2010) 365–375.
[15] A.B. Gaspar, A.M.L. Esteves, F.M.T. Mendes, F.G. Barbosa, L.G. Appel, Appl. Catal. A: Gen. 363 (2009) 109–114.
[16] A.B. Gaspar, F.G. Barbosa, S. Letichevsky, L.G. Appel, Appl. Catal. A: Gen. 380 (2010) 113–117.
[17] J.B. Ko, C.M. Bae, Y.S. Jung, D.H. Kim, Catal. Lett. 105 (2005) 157–161.
[18] H. Oguchi, H. Kanai, K. Utani, Y. Matsumura, S. Imamura, Appl. Catal. A 293 (2005) 64–70.
[19] Z.-Y. Ma, C. Yang, W. Wei, W.-H. Li, Y.-H. Sun, J. Mol. Catal. A: Chem. 231 (2005) 75–81.
[20] K. Tanabe, Mater. Chem. Phys. 13 (1985) 347–364.
[21] W. Hertl, Langmuir 5 (1989) 96–100.
[22] K.T. Jung, A.T. Bell, Catal. Lett. 80 (2002) 63–68.
[23] B.B. Baeza, I.R. Ramos, A. Guerrero-Ruiz, Langmuir 14 (1998) 3556–3564.
[24] M. Mazaheri, M. Valefi, M. Razavi, S.K. Sadrnezhaad, J. Ceram. Int. 35 (2007) 13–20.
[25] W. Widiyastuti, R. Balgis, F. Iskandar, K. Okuyama, J. Chem. Eng. Sci. 65 (2009) 1846–1854.
[26] K.G. Kanade, J.O. Baeg, S.K. Apte, T.L. Prakash, B.B. Kale, J. Mater. Res. Bull. 43 (2008) 723–729.
[27] M. Rezaei, S.M. Alavi, S. Sahebdelfar, Z.-F. Yan, Powder Technol. 168 (2006) 59–63.
[28] V.I. Pârvulescu, H. Bonnemann, V. Pârvulescu, U. Endruschat, A. Rufinska, Ch.W. Lehmann, B. Tesche, G. Poncelet, Appl. Catal. A: Gen. 214 (2001) 273–287.
[29] W.P. Li, S.D. Wang, Int. J. Hydrogen Energy 30 (2005) 973–979.
[30] X. Zheng, C. Yan, R. Hu, J. Li, H. Hai, W. Luo, C. Guo, W. Li, Z. Zhou, Int. J. Hydrogen Energy 37 (2012) 12987–12993.
[31] R. Perez-Hernandez, A.D. Avendano, E. Rosas, V. Rodrıguez-Lugo, Topic Catal. 54 (2011) 572–578.
[32] P. Lopez, G.M. Galicia, M.E. Espinosa-Pesqueira, D. Mendoza-Anaya, Ma.E. Fernandez, A. Gomez-Cortes, J. Bonifacio, G. Martinez-Barrera d, R. Perez-Hernandez, Int. J. Hydrogen Energy 37 (2012) 9018–9027.
[33] A. Szizybalski, F. Girgsdies, A. Rabis, Y. Wang, M. Niederberger, T. Ressler, J. Catal. 233 (2005) 297–307.
[34] S.T. Yong, C.W. Ooi, S.P. Chai, X.S. Wu, Int. J. Hydrogen Energy 38 (2013) 9541–9552.
[35] T.L. Reitz, S. Ahmed, M. Krumpelt, R. Kumar, H.H. Kung, J. Mol. Catal. A: Chem. 162 (2000) 275–285.
[36] T.L. Reitz, P.L. Lee, K.F. Czaplewski, J.C. Lang, K.E. Popp, H.H. Kung, J. Catal. 199 (2001) 193–201.
[37] G.-S. Wu, L.-C. Wang, Y.-M. Liu, Y. Cao, W.-L. Dai, H.-Y. He, K.-N. Fan, Appl. Surf. Sci. 253 (2006) 974–982.
[38] Z.-Y. Ma, C. Yang, W. Wei, W.-H. Li, Y.-H. Sun, J. Mol. Catal. A: Chem. 227 (2005) 119–124.
[39] R. Perez-Hernandeza, G.M. Galicia, D.M. Anaya, J. Palacios, C. Angeles-Chavez, J. Arenas-Alatorre, Int. J. Hydrogen Energy 3 (2008) 4569–4576.
[40] P. Kustowski, L. Chmielarz, R. Dziembaj, P. Cool, E. van Sant, J. Phys. Chem. 109 (2005) 11552–11558.
[41] P. Van der Voort, M. Mitchell, E. Vansant, M. White, Interface Sci. 5 (1997) 169–197.
[42] T. Tsoncheva, L. Ivanova, D. Paneva, I. Mitov, C. Minchev, M. Fröba, Micropor. Mesopor. Mater. 120 (2009) 389–396.
[43] M. Choi, W. Heo, F. Kleitz, R. Ryoo, Chem. Commun. 23 (5) (2000) 349–354.
[44] R.C. Garvie, J. Phys. Chem. 82 (1978) 218–224.
[45] T. Chraska, A.H. King, C.C. Berndt, Mater. Sci. Eng. A 286 (2000) 169–178.
[46] P. Li, I.W. Chen, J.E. Penner-Hahn, JACS 77 (1994) 118–128.
[47] S. Fabris, A.T. Paxton, M.W. Finnis, Acta Mater. 50 (2002) 5171–5178.
[48] R. Burch, A.R. Flambard, J. Catal. 78 (1982) 389–405.
[49] G. Aguila, F. Gracia, J. Cortes, P. Araya, Appl. Catal. B 77 (2008) 325–338.
[50] H. Sahu, G. Rao, Bull. Mater. Sci. 23 (2000) 349–354.
[51] M. Scheithauer, R.K. Grasselli, H. Knözinger, Langmuir 14 (1998) 3019–3029.
[52] A. Bensalem, J.C. Muller, F. Bozon-Verduraz, J. Chem. Soc., Faraday Trans. 88 (1992) 153–154.
[53] H. Sahu, G. Rao, Proc. Indian Acad. Sci. (Chem. Sci.) 113 (2001) 651–658.
[54] L. Chmielarz, P. Kustrowski, R. Dziembaj, P. Cool, E.F. Vansant, Appl. Catal. B: Environ. 62 (2006) 369–380.
[55] A. Kong, H.W. Wang, X. Yang, Y.W. Hou, Y.K. Shan, Micropor. Mesopor. Mater. 118 (2009) 348–353.
[56] S.F. Wang, F. Gu, M.K. Lu, Z.S. Yang, G.J. Zhou, H.P. Zhang, Y.Y. Zhou, S.M. Wang, Opt. Mater. 28 (2006) 1222–1226.
[57] P. Estevesa, Y. Wua, C. Dujardina, M.K. Dongareb, P. Grangera, Catal. Today 176 (2011) 453–457.
[58] A. Patela, P. Shukla, T. Rufford, S. Wang, J. Chena, V. Rudolph, Z. Zhu, Appl. Catal. A: Gen. 409–410 (2011) 55–65.
[59] S. Velu, K. Suzuki, C.S. Gopinath, H. Yoshidac, T. Hattori, Phys. Chem. Chem. Phys. 4 (2002) 1990–1999.
[60] Y. Okamoto, F. Fukino, K. Imanaka, S. Teranishi, J. Phys. Chem. 87 (1983) 3740.
[61] G. Moretti, G. Fierro, M.L. Jacono, P. Porta, Surf. Interface Anal. 14 (1989) 325–336.
[62] R. Dwivedi, A. Maurya, A. Verma, R. Prasad, K.S. Bartwal, J. Alloys Compd. 509 (2011) 6848–6851.

[63] M.C. Biesinger, L.W.M. lau, A.R. Gerson, R.St.C. Smart, Appl. Surf. Sci. 257 (2010) 887–898.
[64] J. Soczyski, R. Grabowski, A. Kozowska, P.K. Olszewski, J. Stoch, Phys. Chem. Chem. Phys. 5 (20) (2003) 4631–4640.
[65] Z. Liu, M. Amiridis, Y. Chen, J. Phys. Chem. B 109 (2005) 1251–1255.
[66] R. Zhou, X. Jiang, J. Mao, X. Zheng, Appl. Catal. A: Gen. 162 (1997) 213–222.
[67] K.V.R. Chary, K.K. Seela, D. Naresh, P. Ramakanth, Catal. Comm. 9 (2008) 75–81.
[68] G. Aguila, J. Jimenez, S. Guerrero, F. Gracia, B. Chornik, S. Quinteros, P. Araya, Appl. Catal. A: Gen. 360 (2009) 98–105.
[69] Y. Zhao, K. Tao, H.L. Wan, Catal. Commun. 5 (2004) 249–252.
[70] S. Esposito, M. Turco, G. Bagnasco, C. Cammarano, P. Pernice, Appl. Catal. A: Gen. 403 (2011) 128–135.
[71] R. Radhakrishnan, J. Wu, S. Jaenicke, G.K. Chuah, ChemCatChem 3 (2011) 761–7707.
[72] F. Ouyang, A. Nakayama, K. Tabada, E. Suzuki, J. Phys. Chem. B 104 (2000) 2012–2018.
[73] R. Pérez-Hernández, A. Gutiérrez-Martínez, C.E. Gutiérrez-Wing, Int. J. Hydrogen Energy 32 (2007) 2888–2894.
[74] B.A. Sexton, Surf. Sci. 88 (1979) 299–318.
[75] I.A. Fisher, A.T. Bell, J. Catal. 184 (1999) 357–376.
[76] T.R. Forrester, R.W. Howe, JACS 109 (1987) 5076–5082.
[77] Y. Jiang, M. Hunger, W. Wang, JACS 128 (2006) 11679–11692.
[78] J.L. White, Catal. Sci. Technol. 1 (2011) 1630–1635.
[79] S.E. Collins, M.A. Baltanas, A.L. Bonivardi, Appl. Catal. A: Gen. 295 (2005) 126–133.
[80] J. Zhu, J.G. van Ommen, L. Lefferts, J. Catal. 225 (2004) 388–397.
[81] F. Zaccheria, N. Scotti, M. Marelli, R. Psaro, N. Ravasio, Dalton Trans. 42 (2013) 1319–1328.
[82] V. Sánchez Escribano, C. del Hoyo Martínez, E. Fernández López, J.M. Gallardo Amores, G. Busca, Catal. Commun. 10 (2009) 861–864.
[83] N. Scotti, M. Dangate, A. Gervasini, C. Evangelisti, N. Ravasio, F. Zaccheria, ACS Catal. 4 (2014) 2818–2826.
[84] G.S. Wu, L.C. Wang, Y.M. Liu, Y. Cao, W.L. Dai, H.Y. He, K.N. Fan, Appl. Surf. Sci. 253 (2006) 974–982.
[85] G.A.M. Hussein, N. Sheppard, M.I. Zaki, R.B. Fahim, J. Chem. Soc. Faraday Trans. 87 (1991) 2655–2659.
[86] K. Takahashi, N. Takezawa, H. Kobayashi, Chem. Lett. 7 (1983) 1061–1064.
[87] S. Lin, D. Xie, H. Guo, J. Mol. Catal. A: Chem. 356 (2012) 165–170.